Energy Engineering

Tech Science Press

Doi:10.32604/ee.2026.076019

ARTICLE

A Control Strategy Leveraging Adaptive Inertia to Enhance Transient Stability of Power Systems Integrated with Grid-Forming Wind Generation

Yuanxiang Luo, Xinmeng Pan* and Xuyang Gao

School of Electrical Engineering, Northeast Electric Power University, Jilin, China

*Corresponding Author: Xinmeng Pan. Email: 15243270592@163.com

Received: 12 November 2025; Accepted: 07 January 2026; Published: 18 June 2026

ABSTRACT: The integration of a high proportion of renewable energy sources via power electronic devices poses significant challenges to power systems. Their grid-connection characteristics differ considerably from those of synchronous generators, leading to a reduction in system inertia. Furthermore, the complex interactions between renewable energy units and the power grid substantially impact the transient stability of the system. Based on the virtual synchronous control characteristics of grid-forming wind turbines (GWT), this paper proposes an adaptive control method to enhance system transient stability. Firstly, a transient stability model for integrating GWT into conventional power systems is established, considering their control structure and typical control strategies. Subsequently, the power interaction mechanism between GWT and synchronous generators is analyzed, revealing the relationship between system stability and the active power control loop of GWT. An improved transient stability assessment index is introduced to quantify the influence of this control loop on system transient stability. Based on this, using the rate of change of virtual rotor speed and the depth of voltage dip as criteria, a flexible inertia control method for grid-forming wind turbines based on adaptive switching of virtual synchronous control is designed, achieving an enhancement in the power system's transient stability. Finally, a simulation model is built on the DIgSILENT/PowerFactory platform. The simulation results demonstrate that the proposed control method effectively suppresses rotor angle instability in synchronous generators and significantly improves the system's transient stability.

KEYWORDS: Grid-forming wind turbine; power angle stability; virtual inertia; adaptive adjustment; transient stability index

1 Introduction

Under the dual challenges of energy problems and environmental pollution, countries around the world have been accelerating the construction and development of new generation power systems in the direction of cleanliness, low carbon and intelligence in recent years [1]. As this transition unfolds, the dynamic characteristics of the power system will undergo a fundamental shift, gradually moving from being dominated by conventional synchronous machines to being governed by the characteristics of converter-interfaced resources [2]. However, the transient stability characteristics of the system are influenced by the combined effects of multiple factors, including the penetration level of power electronics, grid strength, control strategies, and parameter settings [3]. Therefore further increase in the share of renewable energy and power electronic equipment is constrained by the stability of the power system [4]. Under high penetration of renewable energy, the overall system inertia is significantly reduced, leading to weakened frequency regulation capability and increasingly prominent transient stability challenges. To compensate for the lack

of inherent inertia and synchronizing capability in power-electronics-interfaced sources, grid-forming converters have been progressively adopted as an alternative to conventional grid-following control, and have become a key enabling technology for maintaining stable operation of modern power systems. Regarding the impact mechanism of power electronic devices on power system stability, reference [5] analyzed the influence of different control strategies of grid-forming converters on system frequency response, using the frequency nadir and the rate of change of frequency (RoCoF) as quantitative indicators of system frequency.

Reference [6] analyzed that, due to the limited overcurrent capability of converters, grid-forming (GFM) converters enter current-limiting mode during faults, and further examined their post-fault performance. Reference [7] investigates the influence of different control parameters on the transient stability of grid-forming converters, and further provides the transient stability boundaries of these parameters as well as corresponding optimized parameter design methods. However, the above studies mainly focus on the stability of grid-forming converters themselves. With respect to the transient stability of power systems with high penetration of renewable energy. Reference [8] specifically analyzes the transient stability problem associated with wind farm integration into power systems. Reference [9] investigates the impact of the active power recovery rate of a doubly-fed induction generator (DFIG) integrated into a single-machine infinite-bus (SMIB) system on the first-swing rotor angle stability of synchronous generators. It proposes that coordinating and controlling the DFIG's active power recovery process can effectively enhance the transient stability of the power system. Reference [10] evaluates the transient stability of an SMIB system with a single grid-forming converter using a phase-plane approach. Reference [11] models the two-machine system as an equivalent SMIB and employs the extended equal-area criterion to analyze the influence of a direct-drive wind turbine on system stability. Meanwhile, Reference [12] proposed a grid-forming converter integrated into an SMIB system, which enhances overall transient stability by adaptively regulating the active power output of the power-electronics converter; however, large variations in input power may cause the frequency magnitude to exceed prescribed limits.

For the transient stability analysis of multi-machine power systems, Reference [13,14] investigated the two-machine system with a synchronous generator and a virtual synchronous generator (VSG) in parallel and pointed out the effects of inertia, damping and governor on the transient stability of the two-machine system, respectively. Reference [15] thoroughly investigates the impact of renewable energy integration on the rotor-angle stability of multi-machine power systems, considering multiple factors such as the integration location, penetration level, reactive power control strategy, and fault type. References [16,17] employ a small-signal framework centered on eigenvalue analysis to investigate the stability issues in grid-following and grid-forming hybrid systems. Reference [18] provides a critical control scheme for the reliable integration of grid-forming converters into multi-machine power systems, with a focus on its theoretical contributions. Reference [19] develops an adaptive inertia control strategy utilizing system frequency dynamics, effectively damping frequency oscillations, strengthening the grid-supporting capability of wind turbines, and consequently enhancing system frequency stability. Reference [20] proposes an adaptive control strategy based on small-signal modeling and synchronous generator dynamics. By adjusting the virtual inertia and damping coefficient in real time, it effectively suppresses power oscillations and significantly enhances the frequency stability of the system. Reference [21], based on the VSG oscillation-period mechanism, proposes a coordinated adaptive virtual inertia and damping strategy. This strategy reduces transient impact by achieving phase alignment with the reference during mode switching, thereby enhancing frequency stability; however, a systematic discussion regarding its parameter tuning and applicable operational boundaries remains insufficient.

In summary, most existing studies on large-scale renewable energy integration via power electronic devices focus primarily on the device level, with limited attention given to the impact of renewable generation units on the transient stability of the overall power system. In current research on large-scale system transient

stability, grid-following devices remain the main focus, while studies addressing the transient stability of power systems with grid-forming generation units are still lacking.

This paper develops a parallel system model of a grid-forming wind turbine and a synchronous generator, and analyzes the impact of grid-forming wind integration on the electromagnetic power of the synchronous generator based on the nodal-voltage equations. The main contributions of this study are as follows: (1) by applying the equal-area criterion, the changes in the system's transient stability characteristics before and after wind turbine integration are revealed; and a method to enhance transient stability by flexibly tuning the VSG control parameters is proposed. (2) Building on this analysis, an inertia-adaptive switching control strategy is innovatively designed, using voltage sag and the rate of change of angular speed as decision indicators, which effectively improves system transient stability under different fault scenarios. (3) Finally, simulation studies are conducted to verify the correctness and effectiveness of the proposed method, providing new insights for transient stability control of power systems with a high penetration of renewable energy sources.

The remainder of this paper is organized as follows. Section 2 establishes the power system model with a grid-forming wind turbine and analyzes the stability variations before and after its integration. Section 3 presents the design principles of the proposed adaptive virtual inertia control strategy. Section 4 implements the simulation model in DIgSILENT/PowerFactory and evaluates the proposed control strategy using an improved transient stability index. Section 5 concludes the paper and outlines directions for future work.

2 Transient Power-Angle Stability Analysis of Grid-Forming Wind Turbine Access System

2.1 Structure and Control Link of Grid-Forming Wind Turbine

A large share of renewable generation is integrated into the power system via power electronic converters; consequently, its external characteristics are largely determined by the converters' control strategies. Grid-forming converters emulate the rotor-side behavior of synchronous machines by generating reference signals for voltage magnitude and frequency, thereby providing inertia- and damping-like support. This approach is generally more advantageous than conventional control methods when the system accommodates a high penetration of renewables.

Grid-forming control can be categorized into the following methods based on differences in power control loops: sag control, VSG control, matching control [22], etc., compared with the other two control methods VSG can simulate the synchronous generator's rotor equation of motion so that its dynamic response is closer to that of the synchronous generator, so this paper adopts VSG control. Fig. 1 shows the control strategy of VSG control with neglecting damping.

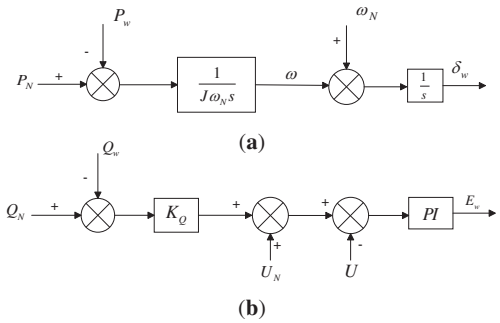

Figure 1: Virtual synchronization control strategy. (**a**) Block diagram of active loop control; (**b**) Block diagram of reactive loop control

Where ω, ω_N denote the virtual angular velocity and rated angular velocity of the converter; P_w, P_N denote the actual and rated values of the active power of the converter; J denotes the virtual inertia, and δ_w denotes the virtual power angle of the output of the active loop; Q_w, Q_N denote the actual and rated values of the reactive power of the converter; U_N, U denote the rated and actual voltage; K_Q denotes the reactive power sag factor; E_w denotes the output voltage of the reactive power control loop. The tuning procedures for all parameters are provided in Appendix A.

2.2 Equivalent External Characteristics of Grid-Connected System for Grid-Forming Wind Turbines

With a large number of renewable energy sources integrated into the power system via power electronic converters, transients associated with converter interfacing exhibit pronounced higher-order nonlinearities and multi-timescale coupling, thereby substantially increasing the complexity of transient stability analysis. To meet this challenge, there is an urgent need to reduce the dimensionality and computational burden of the full-system transient stability analysis by establishing a low-order simplified converter equivalent external characteristic model [12,23]. Fig. 2 illustrates the structure of the virtual synchronous generator (VSG)–controlled grid-forming converter, hereafter referred to as the VSG-GFM.

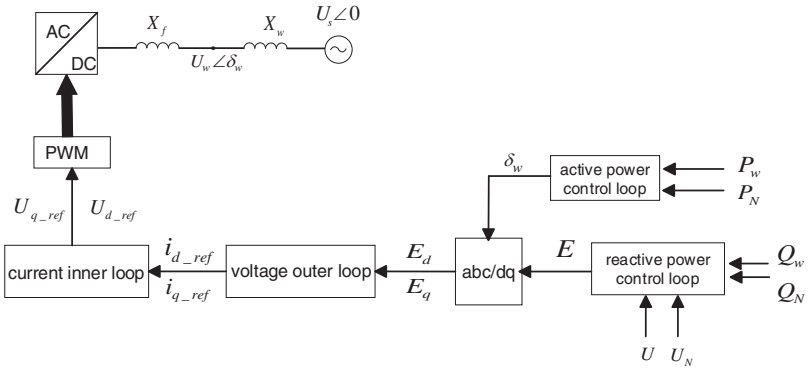

Figure 2: Structure of VSG control grid-type converter

Due to the difference in the response characteristics of the inner and outer rings, the dynamic response of the power outer ring lags behind that of the voltage-current inner ring, so the current inner ring dynamics can be neglected when analyzing the transient synchronous stability problem due to the power ring. The grid-type converter can be equivalent to a controlled voltage source with internal resistance according to its characteristics, and its phase and amplitude can be adjusted to realize the inertia and strength support. Fig. 3 shows its equivalent circuit diagram.

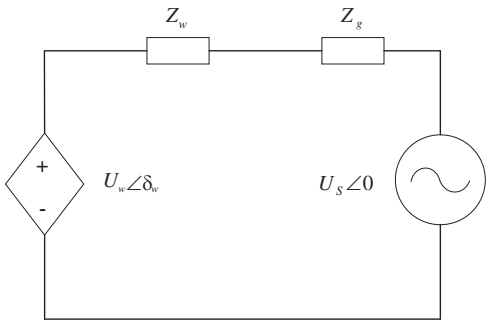

Figure 3: Equivalent circuit diagram

VSG control simulates the swing equation of a synchronous generator, neglecting the damping, its second-order differential equation can be written as:

$$\begin{aligned} \frac{\mathrm{d}\delta_w}{\mathrm{d}t} &= \omega - \omega_N \\ J\frac{\mathrm{d}\omega}{\mathrm{d}t} &= P_N - P_w \end{aligned} \tag{1}$$

where ω, ω_N denote the virtual angular velocity and rated angular velocity of the converter; P_w, P_N denote the actual and rated values of the active power of the converter; J denotes the virtual inertia, and δ_w denotes the virtual power angle of the output of the active loop.

2.3 Transient Stability Analysis of Grid-Type Wind Turbine Connected to a Single Machine Infinity System

For wind turbine access to the power system, modeling methods such as current source, injected power and impedance are often used to characterize the characteristics of the turbine. In this paper, according to the characteristics of virtual synchronous control, the wind turbine model is equivalent to a voltage source model. Fig. 4 shows a grid-forming wind turbine connected to a single-machine infinite-bus (SMIB) system.

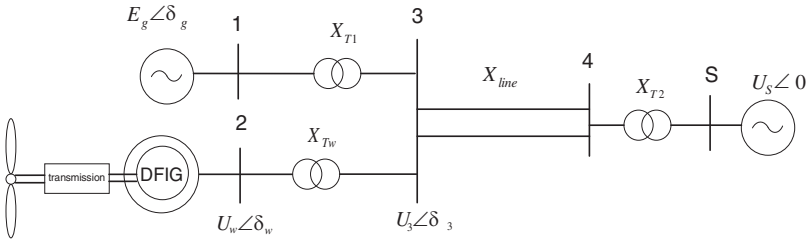

Figure 4: Grid-Forming wind turbine-synchronous generator hybrid system

In the figure, E_g denotes the synchronous generator electromotive force, U_3 denotes the grid-forming point voltage, and U_S denotes the infinity bus voltage. δ_g denotes the synchronous generator power angle, δ_3 denotes the phase of grid-forming point voltage, and the infinity bus denotes set to be the reference phase 0, X_{T1} denotes the reactance of the generator branch step-up transformer, X_{Tw} denotes the total reactance of the grid-constructed wind turbine branch step-up transformer, X_{line} denotes the line reactance, and X_{T2} denotes the step-down transformer reactance.

In the subsequent transient stability analysis, in order not to lose generality, this paper makes the following assumptions:

(1) For the classical second-order model of the synchronous generator, the dynamics of the damping windings are neglected, and the dynamic responses of the governor, the prime mover and the excitation system are not taken into account;
(2) For the influence of current limiting that may occur in power electronic equipment, the current limiting process may not necessarily occur during the transient process, so the influence of the current limiting link of the grid-type converter is ignored;
(3) It is considered that each control link has reached steady state, the parameter design is inductive, and the reactance in the system is much larger than the resistance.

According to the analysis of node voltage equation can be obtained:

$$\begin{bmatrix} Y_1 & 0 & -Y_1 & 0 \\ 0 & Y_2 & -Y_2 & 0 \\ -Y_1 & -Y_2 & Y_1+Y_2+Y_S & -Y_S \\ 0 & 0 & -Y_S & Y_S \end{bmatrix} \begin{bmatrix} E_g \\ U_w \\ U_3 \\ U_S \end{bmatrix} = \begin{bmatrix} I_1 \\ I_2 \\ I_3 \\ I_S \end{bmatrix} \tag{2}$$

where $I1$, $I2$, I_3 and I_S denote the currents injected at nodes 1, 2, 3 and S, respectively, and Y_1, Y_2 and Y_S denote the conductance of the synchronous machine branch, the wind turbine branch, and the common coupling point to the infinity bus, respectively. According to the generator electromagnetic power of the multi-machine system and the derivation of the nodal voltage equations lead to the electromagnetic power of the synchronous generator equation:

$$\begin{aligned} P_{eg} &= \sum_{j=1}^{G} E_i E_j \left[G_{ij} \cos \delta_{ij} + B_{ij} \sin \delta_{ij} \right] \\ &= E_g E_g B_{11} \sin \delta_{gg} + E_g E_w B_{12} \sin \delta_{gw} + E_g U_3 B_{13} \sin \delta_{g3} + E_g U_S B_{1S} \sin \delta_{gS} \\ &= E_g U_3 B_{g3} \sin \delta_{g3} \\ &= \frac{E_g U_w B_{23} B_{13} \sin \delta_{gw}}{B_{13}+B_{23}+B_{3S}} + \frac{E_g U_S B_{13} B_{3S} \sin \delta_g}{B_{13}+B_{23}+B_{3S}} \end{aligned} \tag{3}$$

where: P_{eg} denotes the electromagnetic power output from the synchronous generator, B_{ij} denotes the branch susceptance of the line connecting buses i and j, and δ_{ij} denotes the voltage phase-angle difference between buses i and j.

In order to easily determine the value of the power limit, the above equation is expressed in terms of reactance as:

$$P_{eg} = \frac{X_{3S} E_g U_w}{X_\Sigma} \sin\left(\delta_g - \delta_w\right) + \frac{X'_{23} E_g U_s}{X_\Sigma} \sin \delta_g \tag{4}$$

where $X_\Sigma = X'_{13}X_{3S} + X'_{13}X'_{23} + X'_{23}X_{3S}$; $X'_{13} = X'_d + X_{T1}$; $X'_{23} = X_w + X_{Tw}$; $X_{3S} = X_{Line} + X_{T2}$. X'_d denotes the reactance of the synchronous generator, and X_w denotes the equivalent reactance of the grid-forming wind turbine. In Eq. (4), the first term P_{g1} is the power coupling term, which characterizes the influence of the grid-forming wind turbine on the output power of the synchronous generator, and the second term P_{g2} represents the active power output of the grid-forming system with a single synchronous machine. Where the inertia of the grid-forming wind turbine is smaller than that of the synchronous machine, after a fault occurs, the rotational speed of the grid-forming wind turbine is larger than that of the synchronous generator, and thus $\delta_w > \delta_g$, when $\delta_g = \pi/2$, $\delta_w > \pi/2$, $\sin(\delta_g - \delta_w) < 0$, and $P_{g1} < 0$. The total reactance of the system before connecting the grid-forming wind turbine is $X'_{13} + X_{3S}$, and the reactance in P_{g2} is $\frac{X'_{13}X_{3S}+X'_{13}X'_{23}+X'_{23}X_{3S}}{X'_{23}}$, in order to compare the relative magnitudes of the reactances, the corresponding reactance ratio is evaluated. Based on the basic inequality: $\frac{X'_{13}X'_{23}+X'_{23}X_{3S}}{X'_{13}X_{3S}+X'_{13}X'_{23}+X'_{23}X_{3S}} < 1$, the equivalent system reactance before the grid-connected turbine is interconnected is smaller than the equivalent system reactance after interconnection. Accordingly, $Pg2 < Peg0$, moreover, since $P_{g1} < 0$, superposition gives $P_{g1} + P_{g2} = P_{eg} < P_{eg0}$. Consequently, the amplitude of the power–angle characteristic curve decreases.

As shown in Eq. (3), integrating the wind-turbine network into the system alters the synchronous generator's electromagnetic power. In this paper, the system shown in Fig. 4 is built on the platform of Powerfactory/digsilent, in which: capacity of synchronous machine is 500 mw, the capacity of grid-constructing wind is 230 mw, and the load capacity is 350 mw, the inertia time constant of synchronous generator is T_j = 68 s, and the virtual inertia of the grid-forming wind turbine is J = 20. The three-phase

short-circuit fault occurs at bus 4 in Fig. 4 when t = 0.1 s, and the three-phase short circuit fault is cleared at t = 1.8 s. Fig. 5 shows the power characteristic curve of the synchronous generator before and after the wind turbine is connected.

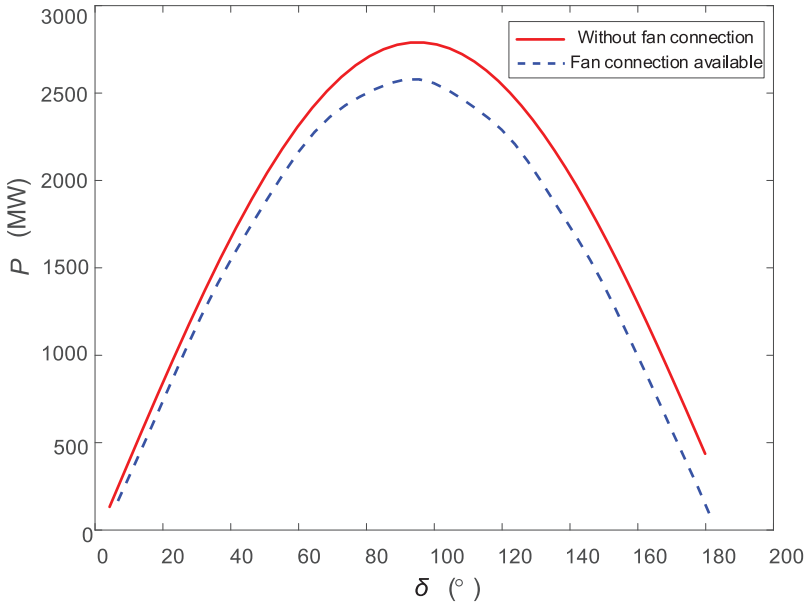

Figure 5: Power angle characteristic curve of synchronous machine before and after wind turbine connection

Fig. 5 shows the power characteristic curves of the synchronous generator before and after the integration of the grid-forming wind turbine. As can be observed from Fig. 5, the integration of the grid-forming wind turbine shifts the synchronous generator's power–angle characteristic curve downward, resulting in a reduced amplitude of the generator's power characteristic curve, which is consistent with the above analysis. Before the grid-forming wind turbine is connected, the power angle at fault clearance is $\delta_{c1} = \delta_{01} + \frac{P_T \Delta t^2}{2T_j}$; the acceleration area is $A_{s1} = (\delta_{c1} - \delta_{01}) \cdot P_T = \frac{P_T^2 \Delta t^2}{2T_j}$, P_T is the mechanical power of the synchronous generator. After the grid-forming GWT are connected to the system, the amplitude of the electromagnetic power of the synchronous generator decreases and the initial power angle increases, resulting in $\delta_{02} > \delta_{01}$, in addition, the power angle at the instant of fault clearance increases, such that $\delta_{c2} > \delta_{c1}$. Since the inertia time constant and mechanical power of the synchronous generator remain constant, the acceleration area remains constant at the same time interval $A'_{s1} = A_{s1}$. Before the access of the GWT, the unstable equilibrium point of the synchronous generator corresponds to the power angle of $\delta_h = \pi - \arcsin(P_m/P_{\max})$, and $\delta_{h2} < \delta_{h1}$, since $P_{\max}$ decreases after the access of the GWT; maximum decelerated area $A_{s2} = \int_{\delta_c}^{\delta_h} (P_e - P_m)\, d\delta$. According to $\delta_{h2} - \delta_{c2} < \delta_{h1} - \delta_{c1}$; $P_{\text{eg}} - P_m < P_{eg0} - P_m$, it can be obtained that the maximum decelerated area A'_{s2} after connecting to the GWT is smaller than that of the previous decelerated area A_{s1}. Thus, the stability margin [24] $\lambda' = \frac{A'_{s2} - A'_{s1}}{A'_{s1}}$, $\lambda = \frac{A_{s2} - A_{s1}}{A_{s1}}$; $\lambda' < \lambda$. It can be seen that the access of GWT leads to a decrease in the stability margin of the system and deteriorates the transient stability of the system. In order to more intuitively describe the impact of GWT accessing the system on the transient stability of the system, this paper adopts the transient stability index (TSI) as the discriminant index of stability [25]:

$$\eta = \frac{\pi - |\Delta\delta_{\max}|}{\pi + |\Delta\delta_{\max}|} \tag{5}$$

where $\Delta\delta_{\max}$ denotes the maximum power angle difference between any two synchronous generators; $\eta > 0$ is transiently stable; $\eta < 0$ indicates transient instability. However, the presence of the grid-forming wind turbine leads to changes in the synchronous generator power characteristic curve, and it is necessary to re-correct its stability threshold.

$$\eta' = \frac{\delta_{correct} - |\Delta\delta_{\max}|}{\delta_{correct} + |\Delta\delta_{\max}|} \tag{6}$$

where δ_{correct} denotes the corrected threshold, given by $\delta_{correct} = \pi - \Delta\delta_g$; $\Delta\delta_g$ denotes the power-angle deviation, defined as $\Delta\delta_g = \delta_g - \delta_{g0}$; δ_{g0} is the generator power angle in the absence of the grid-forming wind turbine, and δ_g is the generator power angle in the presence of the grid-forming wind turbine.

$$\begin{cases} P_w = \frac{E_w U_3}{X_2} \sin\left(\delta_w - \delta_3\right) \\ P_{\text{g}} = \frac{E_g U_3}{X_1} \sin\left(\delta_g - \delta_3\right) \\ P_3 = \frac{U_3 U_S}{X_S} \sin\delta_3 \\ P_3 = P_g + P_w \end{cases} \tag{7}$$

The generator power angle in the absence of the grid-forming wind turbine $\delta_{\text{g0}} = \arcsin\left(\frac{P_{\text{g0}}(X_1+X_S)}{E_g U_\infty}\right)$, and the generator power angle expression in the generator of the grid-forming tubine become $\delta_g = \delta_3 + \arcsin\left(\frac{P_{eg} X_1}{E_g U_3}\right)$, and the value of the power angle cannot be determined because U_3; δ_3; δ_w and δ_g are all variables. Therefore, the following simplifications are made to the system:

(1) The voltage output of the framing grid fan is maintained at the rated value;
(2) The special point is chosen to determine the power angle offset: $P_{\text{g}} = P_{\text{T}}$; $P_{\text{w}} = P_{\text{ref}}$;
(3) Neglect the reactive power influence and only consider the active balance.

Under the simplified assumptions described above, initial guesses are specified for the unknowns U_3, δ_3, δ_w and δ_g, and the resulting nonlinear equations are solved using the Newton–Raphson iterative method. The calculations yield a power-angle offset of $\Delta\delta_g = \delta_g - \delta_{g0} = 5.56°$, and the corrected critical power angle is $\delta_{cr} = 174°$. These results indicate that δ_{cr} decreases; therefore, the integration of the GWT degrades system transient stability.

3 Improved Control Method for System Transient Stability

3.1 The Effect of Virtual Inertia on System Transient Stability

In order to improve the system's transient stability, there are two ideas. The first one can actively reduce the active power reference value of the output power of the grid-configured wind turbine to improve the system stability, but this will reduce the power transfer capability to some extent [26]. The second method is to utilize the characteristics of VSG control to flexibly regulate the control parameters to improve the system's transient stability. From Eq. (1), the following relationship is obtained: $\frac{d\omega}{dt} = \frac{P_N - P_w}{J}$. As the inertia increases, the rate of change of the virtual rotor angular speed decreases, thereby delaying the swing of the virtual power angle of the grid-forming wind turbine. However, excessive inertia causes slow power response in grid-forming wind turbines, leading to adverse interactions with the power angle oscillations of synchronous generators and potentially triggering system oscillations. Fig. 6 illustrates the variations in the phase plane plot under different inertia conditions. It can be observed from the figure that as the virtual inertia of the grid-forming wind turbine increases, the region of stability shrinks, leading to a deterioration in system stability.

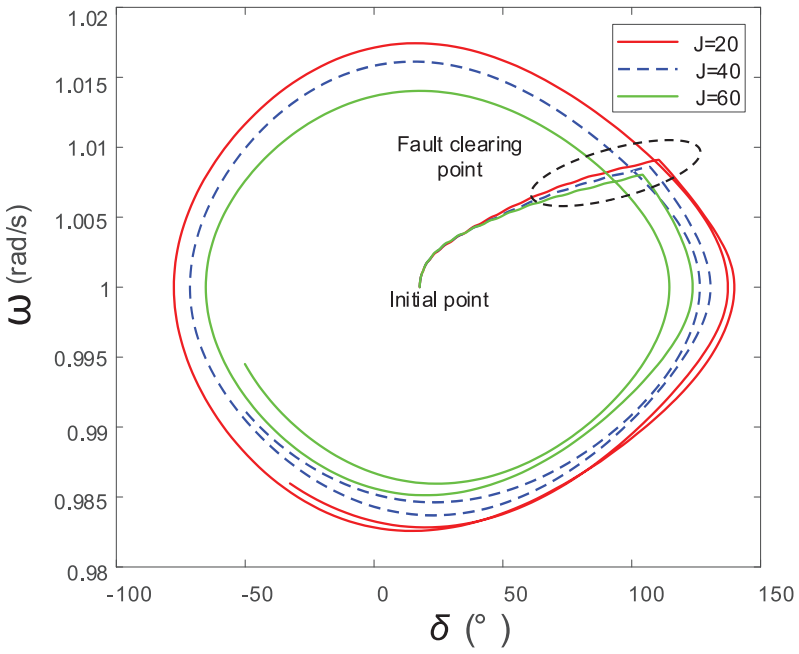

Figure 6: Phase portraits under different inertia conditions

As discussed in Section 2.3, the electromagnetic power of the synchronous machine is related to the virtual power angle of the grid-forming wind turbine. During a fault, the virtual power angle may increase rapidly due to the turbine's low inertia, resulting in an excessively large power-angle deviation between the wind turbine and the synchronous machine. Consequently, the synchronous machine delivers insufficient power during the fault, further enlarging the system's acceleration area.

Considering the dual effects of inertia, this paper leverages the advantages of inertia-flexible control in grid-forming wind turbines with VSG control [27]. By employing an inertia-adaptive control method that dynamically adjusts parameters based on system state, the approach enhances system transient stability. Fig. 7 shows the virtual power angle curve of a grid-forming wind turbine.

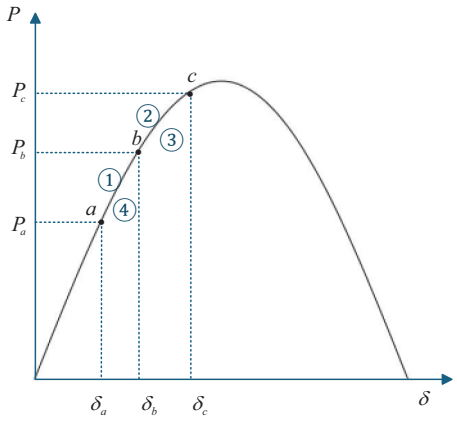

Figure 7: Virtual power angle curves for grid-forming wind turbines

In the interval 1 of Fig. 7: $a \rightarrow b$ for the fault period, the electromagnetic power output of the grid-forming wind turbine is suddenly reduced during the fault period, and the angular velocity of the virtual rotor is accelerated, $\omega_w > \omega_g$, $\mathrm{d}\omega/\mathrm{d}t > 0$, and a larger inertia is needed to prevent the angular velocity from increasing; interval 2: $b \rightarrow c$ for the period of time in which the fault has just been cleared, and although the fault has been cleared, the angular velocity of the virtual rotor at this time is still greater than the synchronous angular velocity, but $\mathrm{d}\omega/\mathrm{d}t < 0$, and at this time the virtual power angle curve should be adjusted to the virtual power angle $\mathrm{d}\omega/\mathrm{d}t$, then a smaller inertia should be used to bring it back to synchronous speed as soon as possible. Interval 3: $c \rightarrow b$, the virtual rotor angular velocity is smaller than the synchronous angular velocity, $\mathrm{d}\omega/\mathrm{d}t < 0$; interval 4: $b \rightarrow a$, for the second swing, at this time the electromagnetic power output of the network fan is greater than the mechanical power.

3.2 Virtual Inertia Adaptive Strategy

As demonstrated by the above analysis, excessively low virtual inertia causes the virtual rotor to spin too rapidly, increasing the rate of change of the power angle and potentially triggering first-swing instability. Conversely, excessively high virtual inertia results in slow virtual rotor speed, preventing timely recovery to synchronous speed after fault clearance. The dynamic response of grid-forming wind turbines can be optimized through flexible inertia control, thereby enhancing system stability.

The formula for traditional inertia adaptive control is as follows:

$$J = \begin{cases} J_0 \frac{\mathrm{d}\omega}{\mathrm{d}t} \leq 0 \cap \Delta U < 0.2 \\ 2J_0 \frac{\mathrm{d}\omega}{\mathrm{d}t} > 0 \cap \Delta U > 0.2 \end{cases} \tag{8}$$

where $\mathrm{d}\omega/\mathrm{d}t$ denotes the rate of change of the virtual rotor angular velocity, ΔU denotes the difference between the rated voltage and the voltage of the low-voltage bus of the step-up transformer of the wind turbine branch of the configuration network [12].

Traditional inertia adaptive control exhibits limitations in certain dynamic control scenarios, lacking inertia values when the angular velocity change rate exceeds zero but the voltage difference falls below 0.2. Existing switching strategies may induce excessive or abrupt inertia transitions, compromising system stability. To address these shortcomings, this paper proposes enhancements to the inertia adaptive control method:

(1) Implementing finer interval segmentation for inertia values, enabling the control system to obtain explicit inertia values under all conditions and enhancing the adaptability and precision of the control method.
(2) Setting optimal inertia values for virtual inertia that match the dynamic performance requirements of different scenarios, thereby limiting inertia variation amplitude and ensuring a smoother, more stable adaptive adjustment process.

During faults, the virtual inertia is set to $J_{\max} = 2J_0$ to reduce the rate of change of the power angle. After fault clearance, it reverts to the smaller inertia J_0, increasing the rate of change of the power angle to rapidly restore synchronous speed. This approach fulfills the requirement for enhanced system transient stability. The improved virtual inertia switching rules are as follows:

$$J = \begin{cases} J_0 \frac{\mathrm{d}\omega}{\mathrm{d}t} \leq 0 \\ 2J_0 \frac{\mathrm{d}\omega}{\mathrm{d}t} > 0 \cap \Delta U > 0.2 \\ J_0 + k \frac{|\omega - \omega_0|}{\omega - \omega_0} \frac{\mathrm{d}\omega}{\mathrm{d}t} \frac{\mathrm{d}\omega}{\mathrm{d}t} > 0 \cap \Delta U < 0.2 \end{cases} \tag{9}$$

where ω denotes the virtual rotor angular speed, ω_0 is the grid angular speed, and K denotes the adjustment coefficient. The system is considered to be in a fault period when $d\omega/dt > 0$ and $\Delta U > 0.2$, and a fault recovery phase when $d\omega/dt < 0$. Considering that the rate of change of the virtual rotor angular velocity can be switched instantaneously at the moment of fault clearing, but the voltage may not be recovered yet. In order to avoid frequent switching of inertia, $d\omega/dt > 0 \cap \Delta U < 0.2$ sets an intermediate value in this case, which can prevent the virtual inertia from changing drastically as well as limit the rate of change of the virtual rotor when it is accelerated in the reverse direction. The switching rule proposed in this paper is based on the assumption of an inductive-dominant grid ($R \ll X$), making it suitable for typical application scenarios such as transmission networks. Further research extending the work to scenarios with high R/X ratios and weak grid conditions is reserved for future studies.

4 Validations

In order to validate the effectiveness of the virtual inertia adaptive method proposed in this paper, we constructed the WTG access to the single machine infinity system and the access to the NEW ENGLAND 10-machine 39-node system on the platform of DIgSILENT/PowerFactory, and carried out simulation experiments. To demonstrate that this strategy can improve the impact on the transient stability of the system due to the access of GWT to the system by increasing the virtual inertia during the fault period.

4.1 Grid-Forming Wind Turbine Integration in a Single-Machine Infinite-Bus System

As previously described, a three-phase short-circuit fault occurs at bus 4 in Fig. 4 at $t = 0.1$ s. Fig. 8 shows the synchronous generator power angle curves for fixed inertia and inertia adaptive methods.

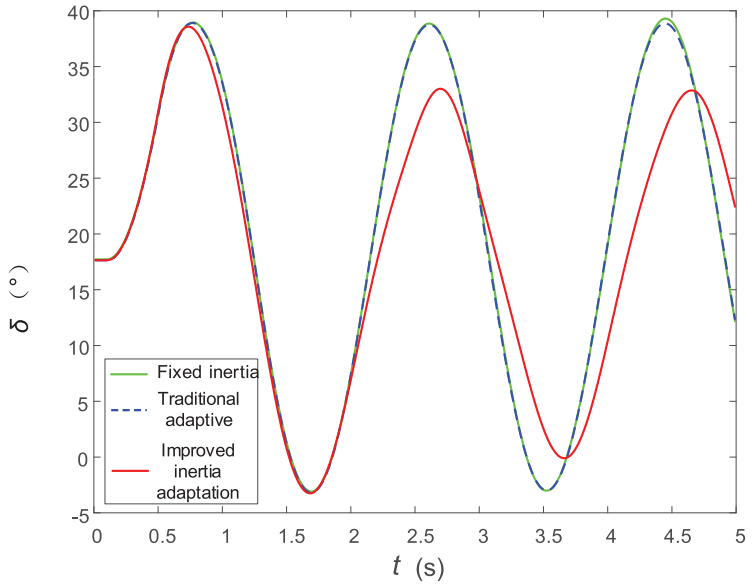

(a)

Figure 8: (Continued)

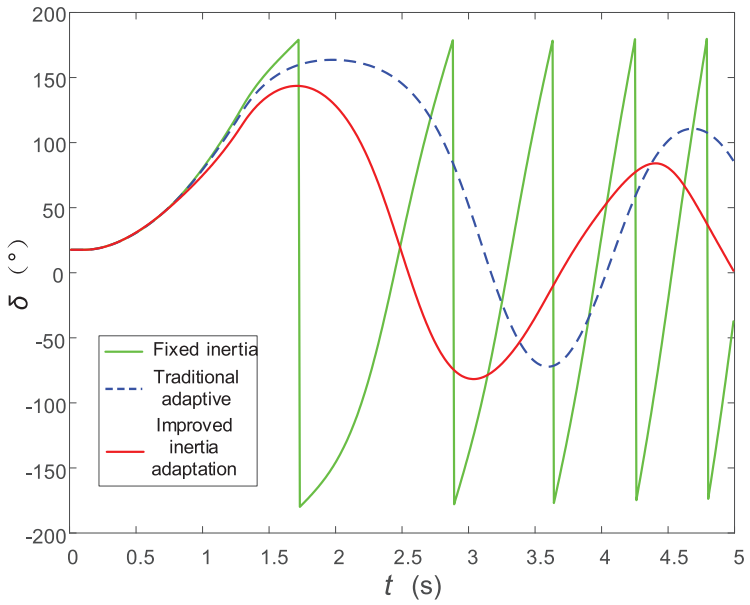

(b)

Figure 8: Power angle curve of synchronous generator. (**a**) Fault clearance within 0.5 s; (**b**) Fault clearance within 1.3 s

As shown in Fig. 8, when the fault is cleared at t = 0.5 s, the power angle fluctuation decreases under the improved inertia adaptation strategy during system stabilization. At t = 1.3 s fault clearance, the fixed inertia system enters an unstable state, whereas the improved inertia adaptation strategy restores the synchronous generator's power angle stability while reducing its fluctuation amplitude compared to conventional inertia adaptation control methods. Fig. 9 shows the angular frequency throughout the fault process of the wind turbine under three inertia conditions.

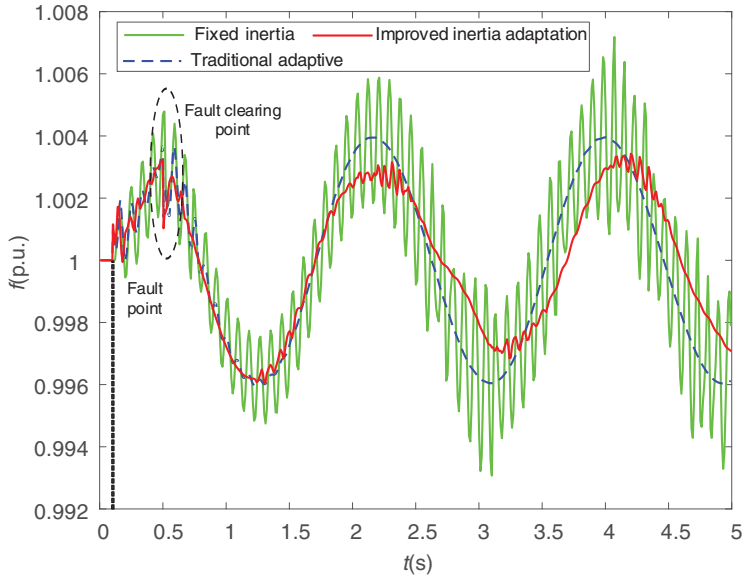

(a)

Figure 9: (Continued)

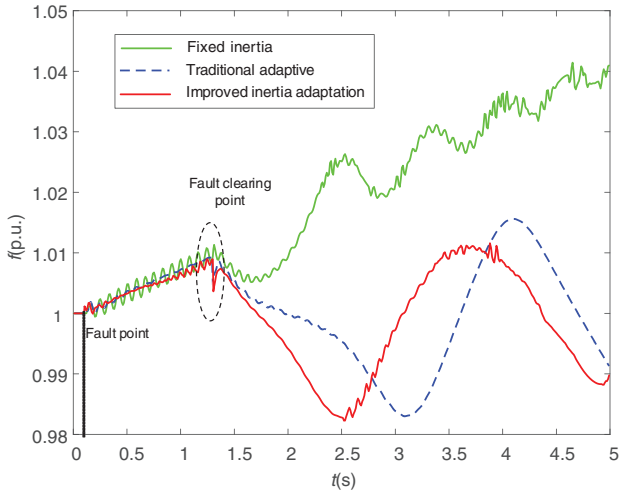

(b)

Figure 9: Wind turbine generator angular frequency. (**a**) Fault clearance within 0.5 s; (**b**) Fault clearance within 1.3 s

Fig. 9 demonstrates that the inertia adaptation strategy suppresses frequency rise in wind turbines when the fault is cleared at t = 0.5 s. At t = 1.3 s, the wind turbines transition from an unstable to a stable state. Regardless of whether the system is stable or unstable, the improved inertia adaptation control strategy outperforms the traditional inertia adaptation approach. The enhanced inertia adaptive strategy not only improves system transient stability but also enhances the transient stability of the wind turbine itself.

4.2 Grid-Forming Wind Turbine Integration in the New England 10-Machine 39-Bus System

Fig. 10 shows that the GWT are connected to the bus 23 in the NEW ENGLAND 10-machine 39-node system, the synchronous generator G2 is the balancing node, the total capacity of synchronous machine is 5326 MW, the total capacity of GWT is 2500 MW, and the load capacity is 6097.1 MW. t = 0.1 s a three-phase short-circuit fault occurs at bus 16, and the fault is cleared at t = 0.24 s.

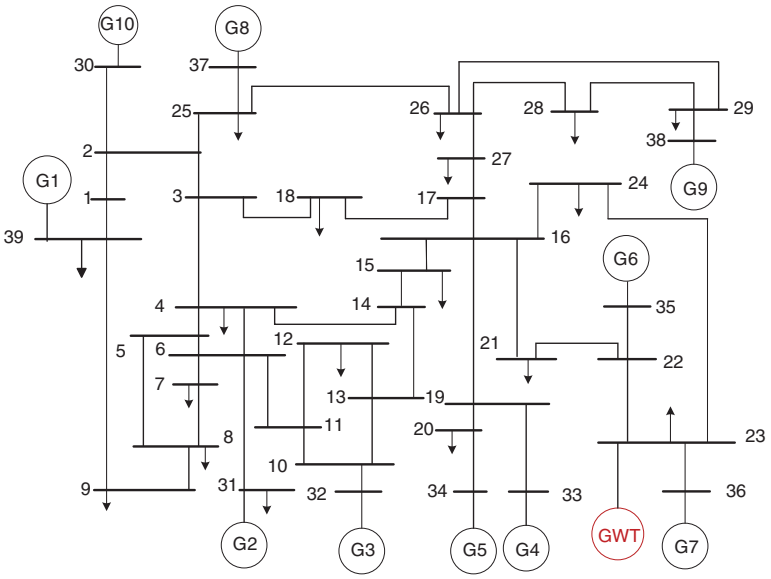

Figure 10: Integration of grid-forming wind turbines into the New England ten-machine thirty-nine node system

Fig. 11 shows the power angle curves of each synchronous generator when different inertia control methods are applied in a ten-machine system. Under identical fault clearance times, the power angle curves using the traditional inertia adaptive control method show improved stability compared to fixed inertia but still exhibit instability tendencies. In contrast, the modified inertia adaptive strategy keeps the power angles of all synchronous generators within bounded ranges.

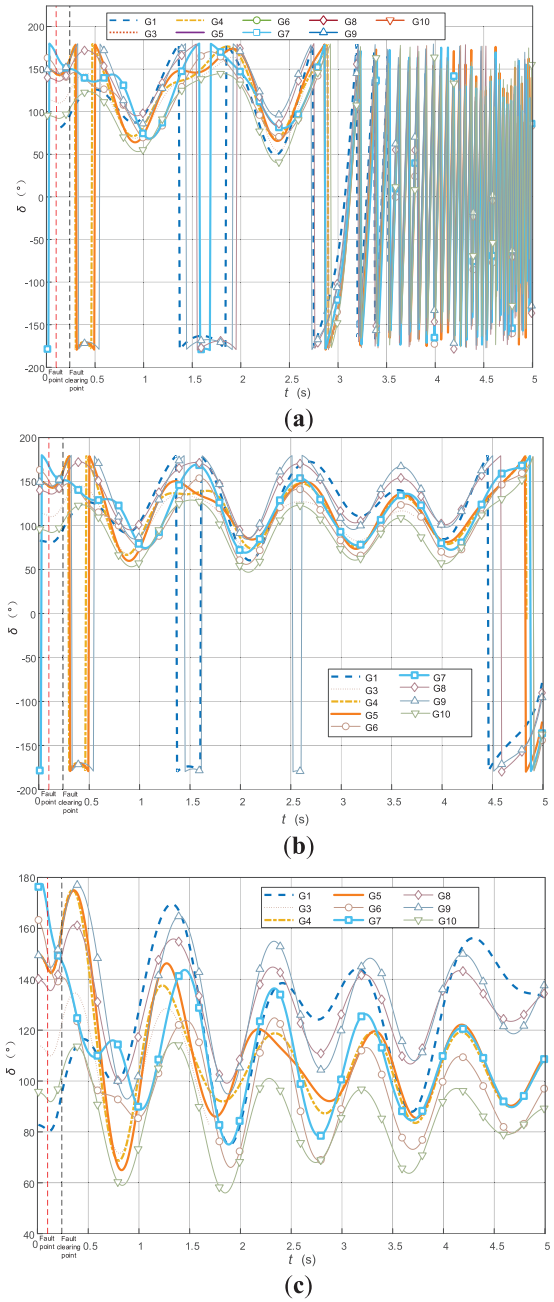

Figure 11: Power angle curves for each synchronous generator. (**a**) The wind turbine employs a fixed inertia strategy to clear the fault at t = 0.24 s; (**b**) The wind turbine employed a traditional inertia-adaptive strategy and cleared the fault at t = 0.24 s; (**c**) The wind turbine employed an improved inertia adaptive strategy to clear the fault at t = 0.24 s

Fig. 12 displays the frequency response of the wind turbine throughout the entire fault process within a multi-machine system. As shown in Fig. 12, the improved inertia-adaptive strategy effectively suppresses the instability of the wind turbine, restoring it to a stable operating state. Table 1 shows the TSIs corresponding to different fault locations for the case of grid-constructed wind turbines connected to a single machine infinity system as well as a multi-machine system, respectively.

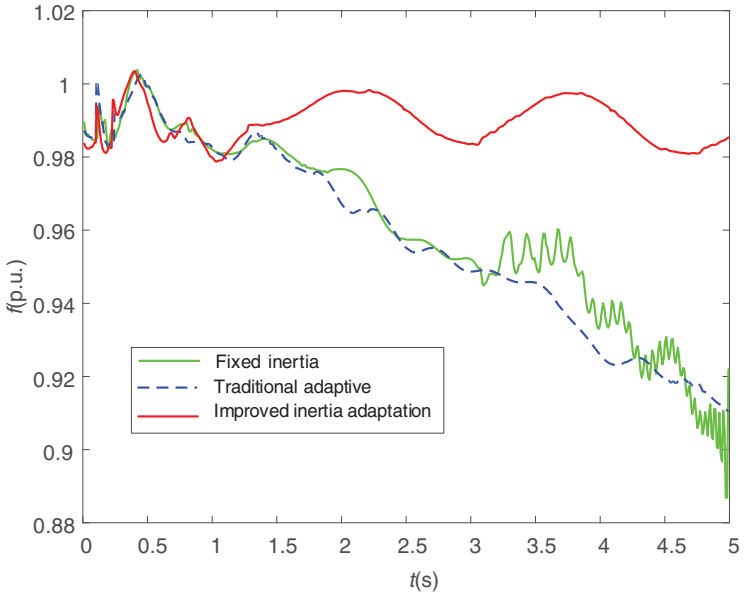

Figure 12: Wind turbine generator angular frequency

Table 1: Comparison between this study and previous research

Reference	Research focus	Typical system	SG–GFM parallel system	Node-voltage-based/Analytical impact on SG electromagnetic power P_e	EAC-based transient stability interpretation	Parameter-tuning principle for transient stability improvement	Adaptive inertia switching
[5]	Frequency stability	Low-inertia grid	√	–	–	Δ	–
[10]	Transient stability	Voltage sag	–	–	–	√	–
[12]	Transient stability limit enhancement	Converter–SG parallel	√	Δ	√	√	–
[20]	Adaptive VSG control	Inertia–damping tuning	–	–	–	√	Δ
Proposed	Transient stability improvement	GWT–SG parallel	√	√	√	√	√

Note: *Symbols: √: explicitly addressed as a main contribution; Δ: discussed but not central or not fully quantified; —: not addressed.

In Table 2: η'_1, η'_2, and η'_3 denote the TSI values obtained using three different inertia control methods for a grid-forming wind turbine integrated into the single-machine infinite-bus system and the multi-machine system, respectively, under different fault locations.

Table 2: Comparison results of the transient stability index

Fault location	Grid-type wind turbine connected to single machine infinity system		Grid-type wind turbine connected to NEW ENGLAND 10-machine 39-node system	
	BUS3	BUS2	BUS16	BUS21
Fixed inertia	$\eta'_1 = 0.608$	$\eta'_1 = 0.665$	$\eta'_1 = -0.347$	$\eta'_1 = -0.346$
Traditional adaptive	$\eta'_2 = 0.610$	$\eta'_2 = 0.672$	$\eta'_2 = -0.345$	$\eta'_2 = -0.329$
Inertia adaptive	$\eta'_3 = 0.637$	$\eta'_3 = 0.681$	$\eta'_3 = 0.481$	$\eta'_3 = 0.143$

The higher the system stability, the greater its corresponding TSI value. As shown in the table data, the system's TSI values are consistently higher when employing the improved inertia adaptation strategy compared to using fixed inertia. Therefore, adopting the improved adaptive inertia significantly enhances system stability. Based on the simulation results in Figs. 11 and 12 and the comparative data in Table 2, it is evident that the proposed improved inertia adaptation strategy for enhancing system transient stability is also applicable in complex multi-machine systems.

5 Conclusion

A large number of new energy sources are connected to the system through power electronic equipment, which changes the transient stability of the system. In this paper, by analyzing the control links and external characteristics of the grid-connected turbines, we study the impact on transient stability due to the grid-connected turbines' access to the system, and use voltage dips and the rate of change of angular velocity, and apply inertia adaptive strategy to the grid-forming wind turbines, so as to realize the improvement of the system's transient stability. This paper mainly draws the following conclusions:

(1) This paper analyzes the control link of the grid-forming wind turbine to obtain its equivalent voltage source model, and then gives the changes of the node voltage equations in the system after its access to the power system, combined with the power angle characteristic curve of the synchronous generator. It is concluded that the access of the grid-forming wind turbine deteriorates the transient stability of the system.

(2) Since the network fan adopts VSG control, its virtual inertia can be flexibly regulated according to the system needs. Therefore, this paper adopts the voltage sag and the rate of change of angular velocity as control criteria. During the fault period, the virtual inertia of the grid-forming wind turbine is increased to suppress the rapid growth of its virtual power angle. During fault recovery, the virtual inertia is reduced so that the virtual power angle can return rapidly to the synchronous speed. This strategy not only improves the transient stability of the network turbine itself, but also improves the transient stability of the overall system; it effectively prevents the transient instability of the system caused by new energy access to the system under large disturbances.

(3) This paper demonstrates the effectiveness of the proposed strategy using the transient stability index. In the single-machine system, when a three-phase short-circuit fault occurs at $t = 0.1$ s and is cleared at $t = 0.5$ s, the TSI values for the fixed-inertia and conventional adaptive inertia schemes are 0.608

and 0.610, respectively, while the proposed adaptive strategy increases the TSI to 0.637, significantly enhancing the transient stability margin. Meanwhile, the maximum frequency deviation is reduced to 0.007, which is notably lower than the 0.009 of the conventional scheme and the 0.014 of the fixed-inertia scheme. In the NEW ENGLAND 10-machine 39-bus system, under the same fault condition, the TSI values for the fixed-inertia and conventional adaptive schemes are −0.347 and −0.345, respectively, both indicating transient instability. In contrast, the proposed adaptive strategy raises the TSI to 0.481, enabling the system to transition from instability to maintained transient stability under equally severe disturbances. The maximum frequency deviation is also markedly reduced—from 0.116 (fixed inertia) and 0.093 (conventional scheme) to 0.024. These results demonstrate that the proposed strategy not only outperforms both the fixed-inertia and conventional adaptive schemes, but also achieves the critical improvement from "unstable to stable" in a multi-machine system, thereby effectively enhancing the transient stability of the power system under large disturbances.

Although this study proposes an adaptive inertia control strategy based on voltage sag and the rate of change of angular velocity, which effectively enhances the system's transient stability under large disturbances, there remain several directions worthy of further in-depth investigation. To maintain model generality, the grid-forming wind turbine is moderately simplified, and the dynamic current-limiting mechanism that may be activated in its converter during severe disturbances is not considered. Future work will focus on investigating the impacts of current-limiting dynamics on system transient behavior using more detailed models, validating the applicability of the proposed strategy under unbalanced faults and weak-grid conditions, and further exploring how multi-source coordinated control can improve transient stability in hybrid systems comprising grid-following wind turbines, grid-forming wind turbines, and synchronous machines. These topics will constitute the main focus of our subsequent research.

Acknowledgement: Not applicable.

Funding Statement: This work was supported by National Natural Science Foundation of China (52377082).

Author Contributions: Yuanxiang Luo provided the conceptual framework for this research. Xinmeng Pan proposed the key methodology, completed simulation verification, and authored and integrated the entire manuscript. Xuyang Gao performed meticulous grammatical proofreading. All authors participated in revising the manuscript and reviewing its content. All authors reviewed and approved the final version of the manuscript.

Availability of Data and Materials: The data that support the findings of this study are available from the corresponding author, upon reasonable request.

Ethics Approval: Not applicable.

Conflicts of Interest: The authors declare no conflicts of interest.

Nomenclature

Abbreviations

GWT	Grid-Forming wind turbines
RoCoF	Rate of change of frequency
VSG	Virtual synchronous generator
GFM	Grid-Forming
TSI	Transient stability index
PWM	Pulse width modulation
DFIG	Doubly fed induction generator
SG	Synchronous generator

EAC	Equal area criterion

Parameters

ω	Virtual angular velocity of the converter
ω_N	Rated angular velocity of the converter
P_w	Actual active power of the converter
P_N	Rated active power of the converter
J	Virtual inertia
δ_w	Virtual power angle from the active power control loop
Q_w	Actual reactive power of the converter
Q_N	Rated reactive power of the converter
U_N	Rated voltage
U	Actual voltage
K_Q	Reactive power droop coefficient
E_w	Output voltage of the reactive power control loop
X_w	Equivalent reactance between the point of common coupling and the infinite bus
δ_c	Critical clearing angle
X_f	Filter inductor
U_s	Infinite bus voltage
E_d	d-axis voltage
E_q	q-axis voltage
i_{d_ref}	d-axis current reference
i_{q_ref}	q-axis current reference
U_{d_ref}	d-axis voltage reference
U_{q_ref}	q-axis voltage reference
Z_w	Equivalent impedance from the grid-forming wind turbine to the PCC
Z_g	Equivalent impedance between the point of common coupling and the infinite bus
E_g	Electromotive force of a synchronous generator
δ_g	Rotor angle of synchronous generator
U_3	Voltage at PCC
δ_3	Voltage phase angle at PCC
X_{T1}	Reactance of the step-up transformer in the generator branch
X_{Tw}	The total reactance of the grid-forming wind turbine step-up transformer branch
X_{line}	Line reactance
X_{T2}	Reactance of step-down transformer
P_{eg}	Electromagnetic power
P_T	Mechanical power
$P_{\max}$	Maximum electromagnetic power
T_j	Inertia time constant
δ_0	Initial power angle
δ_h	Maximum swing angle

Appendix A

The control system in this study is tuned using a hierarchical cascaded procedure. First, the inner current loop is tuned under the constraints imposed by the PWM and sampling frequencies to achieve the highest closed-loop bandwidth. Then, with the current loop closed, the outer voltage loop is tuned such that its bandwidth is significantly lower than that of the current loop. Finally, the VSG active/reactive power outer loops are tuned with the lowest bandwidth to ensure decoupling from the voltage loop. To avoid loop interaction, the crossover frequencies of adjacent loops are selected to differ by at least a factor of five.

As can be seen from Fig. 1a:

$$J\omega_N \frac{d\Delta\omega}{dt} = P_N - P_w, \frac{d\delta}{dt} = \omega, \Delta\omega = \omega - \omega_N \tag{A1}$$

The equivalent grid-connected power–angle relationship can be linearized under small-signal perturbations as:

$$P_N \approx \frac{EU_g}{X_{eq}} \sin\delta_w \Rightarrow P_N \approx K_s\Delta\delta, K_s = \frac{EU_g}{X_{eq}} \cos\delta_0 \tag{A2}$$

A commonly used approximation in the vicinity of the rated operating point is: $E \approx U_g \approx U_N, \delta_0 \approx 0$.

$$K_s = \frac{U_N^2}{X_{eq}}, X_{eq} = X_f + X_w \tag{A3}$$

By combining the above, the second-order rotor-angle dynamics can be obtained, and the corresponding natural frequency is approximately:

$$\omega_{n,p} \approx \sqrt{\frac{K_s}{J\omega_N}} \tag{A4}$$

Therefore, J can be calculated as:

$$J = \frac{K_s}{\omega_N \omega_{n,p}^2} \tag{A5}$$

According to Fig. 1b, we obtain:

$$U^* = U_N + K_Q(Q_N - Q_w), eU = U^* - U \tag{A6}$$

The PI controller output is E_w, which is then fed into the voltage outer loop shown in Fig. 2. Let the allowable voltage deviation be ΔU. Under grid-connected operation, the available reactive power range is $\pm Q_{\max}$ (determined by the converter current limit and the operating point). Then:

$$K_Q = \frac{\Delta U_{\max}}{Q_{\max}} \tag{A7}$$

PI tuning: Based on the already tuned inner current loop and outer voltage loop, a small step is applied to the $E_w \rightarrow U$ path to obtain an equivalent first-order model:

$$G_u(s) = \frac{k_u}{\tau_u s + 1} \tag{A8}$$

The desired closed-loop bandwidth of the reactive power outer loop, $\omega_{c,q}$, is selected (satisfying $\omega_{c,q} \ll \omega_{cv}$), and the damping ratio ζ_q is chosen (typically in the range 0.6–1.0). The PI parameters are then obtained via pole placement as:

$$K_{p,q} = \frac{2\zeta_q\omega_{c,q}\tau_u - 1}{k_u}, k_{i,q} = \frac{\omega_{c,q}^2\tau_u}{k_u} \tag{A9}$$

$\omega_{c,q}$ should be selected such that $2\zeta_q\omega_{c,q}\tau > 1$ to ensure $K_{p,q} > 0$.

References

1. IRENA. Global renewables outlook: energy transformation 2050. Abu Dhabi, United Arab Emirates: International Renewable Energy Agency; 2020.
2. Poulose A, Kim S. Transient stability analysis and enhancement techniques of renewable-rich power grids. Energies. 2023;16(5):2495. doi:10.3390/en16052495.
3. Ratnam KS, Palanisamy K, Yang G. Future low-inertia power systems: requirements, issues, and solutions—a review. Renew Sustain Energy Rev. 2020;124:109773. doi:10.1016/j.rser.2020.109773.
4. Sajadi A, Kolacinski RM, Clark K, Loparo KA. Transient stability analysis for offshore wind power plant integration planning studies: part I: short-term faults. IEEE Trans Ind Appl. 2019;55(1):182–92. doi:10.1109/TIA.2018.2868550.
5. Tayyebi A, Gross D, Anta A, Kupzog F, Dorfler F. Frequency stability of synchronous machines and grid-forming power converters. IEEE J Emerg Sel Topics Power Electron. 2020;8(2):1004–18. doi:10.1109/jestpe.2020.2966524.
6. Fan B, Wang X. Fault recovery analysis of grid-forming inverters with priority-based current limiters. IEEE Trans Power Syst. 2023;38(6):5102–12. doi:10.1109/TPWRS.2022.3221209.
7. Ge P, Tu C, Xiao F, Guo Q, Gao J. Design-oriented analysis and transient stability enhancement control for a virtual synchronous generator. IEEE Trans Ind Electron. 2023;70(3):2675–84. doi:10.1109/TIE.2022.3172761.
8. Tsourakis G, Nomikos BM, Vournas CD. Contribution of doubly fed wind generators to oscillation damping. IEEE Trans Energy Convers. 2009;24(3):783–91. doi:10.1109/TEC.2009.2025330.
9. Munkhchuluun E, Meegahapola L, Vahidnia A. Impact of active power recovery rate of DFIG wind farms on first swing rotor angle stability. IET Generation Trans Dist. 2020;14(25):6041–8. doi:10.1049/iet-gtd.2020.1072.
10. Xiong X, Wu C, Blaabjerg F. Effects of virtual resistance on transient stability of virtual synchronous generators under grid voltage sag. IEEE Trans Ind Electron. 2022;69(5):4754–64. doi:10.1109/TIE.2021.3082055.
11. Liu Z, Liu C, Li G, Liu Y, Liu Y. Impact study of PMSG-based wind power penetration on power system transient stability using EEAC theory. Energies. 2015;8(12):13419–41. doi:10.3390/en81212377.
12. Liang S, Yao LZ, Xu J, Cheng F, Yu HN, Deng JL, et al. Power system transient stability limit enhancement method based on virtual synchronous grid-forming control of power electronic converters. Proc CSEE. 2025;45(8):2911–25. (In Chinese). doi:10.13334/j.0258-8013.pcsee.232381.
13. Cheng H, Shuai Z, Shen C, Liu X, Li Z, Shen ZJ. Transient angle stability of paralleled synchronous and virtual synchronous generators in islanded microgrids. IEEE Trans Power Electron. 2020;35(8):8751–65. doi:10.1109/TPEL.2020.2965152.
14. Shi K, Song W, Ge H, Xu P, Yang Y, Blaabjerg F. Transient analysis of microgrids with parallel synchronous generators and virtual synchronous generators. IEEE Trans Energy Convers. 2020;35(1):95–105. doi:10.1109/TEC.2019.2943888.
15. Rezaei J, Golshan MEH, Alhelou HH. Impacts of integration of very large-scale photovoltaic power plants on rotor angle and frequency stability of power system. IET Renew Power Gener. 2022;16(11):2384–401. doi:10.1049/rpg2.12529.
16. Benedetti L, Paspatis A, Papadopoulos PN, Egea-Àlvarez A, Hatziargyriou N. Investigation of grid-forming and grid-following converter multi-machine interactions under different control architectures. Electr Power Syst Res. 2024;234(7):110813. doi:10.1016/j.epsr.2024.110813.
17. Wang Y, Ruan L, Yang M, Xiao X, Chen S, Gomis-Bellmunt O. Control interaction analysis of hybrid system with grid-following and grid-forming inverters based on admittance decomposition. Int J Electr Power Energy Syst. 2024;162(1):110267. doi:10.1016/j.ijepes.2024.110267.
18. Chen J, Prystupczuk F, O'Donnell T. Use of voltage limits for current limitations in grid-forming converters. CSEE J Power Energy Syst. 2020;6(2):259–69. doi:10.17775/CSEEJPES.2019.02660.
19. Sato T, Alsharif F, Umemura A, Takahashi R, Tamura J. Stability improvement of power system by cooperative virtual inertia control and reactive power control of PMSG wind generator and battery. Electr Eng Jpn. 2022;215(1):e23362. doi:10.1002/eej.23362.
20. Xia Y, Wang Y, Chen Y, Shi J, Yang Y, Li W, et al. A cooperative adaptive VSG control strategy based on virtual inertia and damping for photovoltaic storage system. Energies. 2025;18(6):1505. doi:10.3390/en18061505.

21. Shi T, Sun J, Han X, Tang C. Research on adaptive optimal control strategy of virtual synchronous generator inertia and damping parameters. IET Power Electron. 2024;17(1):121–33. doi:10.1049/pel2.12620.
22. Zhang H, Xiang W, Lin W, Wen J. Grid forming converters in renewable energy sources dominated power grid: control strategy, stability, application, and challenges. J Mod Power Syst Clean Energy. 2021;9(6):1239–56. doi:10.35833/MPCE.2021.000257.
23. Wang X, Taul MG, Wu H, Liao Y, Blaabjerg F, Harnefors L. Grid-synchronization stability of converter-based resources—an overview. IEEE Open J Ind Appl. 2020;1:115–34. doi:10.1109/OJIA.2020.3020392.
24. Wang Q, Xue AC, Zheng YJ, Bi TS. Analysis of the impact of doubly-fed wind power centralized access on transient power angle stabilization. Power Syst Technol. 2016;40(3):875–81. (In Chinese). doi:10.13335/j.1000-3673.pst.2016.03.031.
25. Ji KX, Qiao J, Zhao ZX, Zhao JM, Shi MJ, Yang F. Adaptive assessment of power system transient stability considering sample distribution imbalance. Power Power Syst Technol. 2025;49(6):2302–10. (In Chinese). doi:10.13335/j.1000-3673.pst.2024.0812.
26. Wang L, Hu P, Zhang W. A current limiting strategy for grid-forming converters based on voltage deviation adaptive virtual impedance. Int J Electr Power Energy Syst. 2025;173(3):111356. doi:10.1016/j.ijepes.2025.111356.
27. Li K, Wei Y, Zhang J. Adaptive virtual synchronous generator control strategy based on frequency integral compensation. Electronics. 2024;13(21):4318. doi:10.3390/electronics13214318.